Inorganic Chemistry

Article

pubs.acs.org/IC

Diverse Self-Assembly from Predesigned Conformationally Flexible Pentanuclear Clusters Observed in a Ternary Copper(II)–Triazolate–Sulfoisophthalate System: Synthesis, Structure, and Magnetism

En-Cui Yang,* Yuan-Yuan Zhang, Zhong-Yi Liu, and Xiao-Jun Zhao*

College of Chemistry, Key Laboratory of Inorganic-Organic Hybrid Functional Material Chemistry, Ministry of Education, Tianjin Key Laboratory of Structure and Performance for Functional Molecules, Tianjin Normal University, Tianjin 300387, People's Republic of China

Supporting Information

ABSTRACT: Self-assembly from the predesigned Cu^{II}_5 secondary building unit (SBU) in the ternary Cu^{II}–triazolate–sulfoisophthalate system generates three interesting magnetic samples: an open pillared-layer framework with nanosized Cu^{II}_{30} metallamacrocycle-based sublayer (**1**), a (3,6)-connected 2-fold interpenetrating network consisting of alternating Cu^{II}_5 and Cu^{II}_1 cores (**2**), and a (4,8)-connected architecture constructed from centrosymmetric Cu^{II}_7 clusters and four-branched 5-sulfoisophthalate (sip^{3-}) connectors (**3**). These various structures significantly result from the variable connectivity and the slight expansion of the predetermined conformationally flexible Cu^{II}_5 SBUs. Furthermore, these intriguing structural motifs in **1**–**3** essentially induce different magnetic phenomena. A field-dependent metamagnetic transition from antiferromagnetic ordering to weak ferromagnetism is observed in the frustrated Cu^{II}_{30}-based sublayer of **1**. The paramagnetic Cu^{II}_1 core in **2** virtually contributes to an $S = {}^1/_2$ spin ground state due to the completely compensated magnetic moment in the 1,2,3-triazolate (ta^-)-bridged Cu^{II}_5 cluster containing ribbon. In contrast, strong antiferromagnetic interactions in the locally centrosymmetric Cu^{II}_7 cluster lead to an overall $S = {}^1/_2$ spin ground state of **3**. Thus, the SBU-derived self-assembly strategy provides important hints for polymetallic cluster based high-dimensional magnetic materials, which also brings a new vision for the design and construction of novel functional materials.

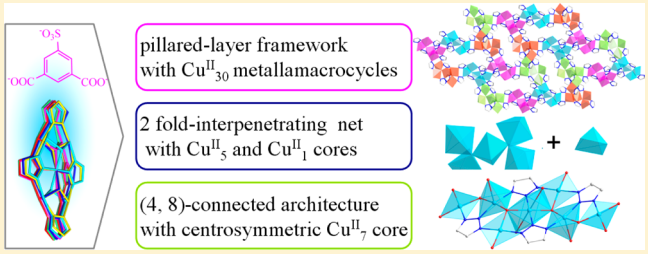

INTRODUCTION

One of the most important goals in the preparations of new functionalized materials is to achieve the real "design" and to obtain tailor-made samples with expected structures and properties starting from well-characterized inorganic and organic precursors.[1] However, it is still quite challenging to fabricate high-nuclearity (>5) cluster-based magnetic entities because of the difficult controls over the size, nuclearity, and intercluster connection mode. In fact, a secondary building unit (SBU) that possesses a relatively stable component, a specific geometric shape, and the desired directionality[2] could be promisingly used to make extended functional frameworks. Recent studies have shown that triazole and its diverse derivatives can easily generate various recurring SBUs by a subtle choice of the reaction system and appropriate manipulations of the synthetic conditions.[1−20] The commonly observed SBUs in these systems usually consist of butterfly-shaped M^{II}_4 cores (M = Cu, Co, Mn),[1,9] metal ion centered MZn_4 tetrahedron subunits (M = Zn, Ru, Cd, Fe, Co, Ni, Cu),[10−15] and approximately coplanar M^{II}_5 (M = Zn, Cu, Co) clusters composed of two corner-sharing triangles.[13,16,17] Unfortunately, in comparison with the conventional bottom-up synthesis, exploration of the self-assembly technique starting from the SBU is currently limited,[21] especially for polymetallic cluster based three-dimensional (3D) magnetic entities. Herein, utilizing a predetermined $[Cu_5(\mu_3\text{-}OH)_2(ta)_4]^{4+}$ cluster as a SBU and an anionic sip^{3-} ligand as an organic linker (ta^- = 1,2,3-triazolate and sip^{3-} = 5-sulfoisophthalate), we carried out coordination-driven assembly reactions in the ternary Cu^{II}–triazolate–sip^{3-} system by triggering external reaction conditions. The Cu^{II}_5 cluster can be easily generated as long as the μ_3-ta^- ligand and the μ_3-OH^- group coexist in the same system,[13,16,17] and other particular reasons for such a choice are also based on the following considerations. An inorganic Cu^{II} ion with an unpaired d electron can adopt diversely stable coordination spheres (such as tetrahedral, square-planar, trigonal-bipyramidal, square-pyramidal, and octahedral geometries), which can effectively adjust the symmetry, conformation, and coplanarity of the predesigned SBU, meeting the requirements of the aggregate process and simultaneously contributing to the magnetic superexchange couplings. On the other hand, a rigid sip^{3-} ligand that is modified by three tunable binding groups can behave as a polytopic connector and enrich the linkages of the predesigned SBUs responsible for the network diversity. As a result, three Cu^{II}_5 SBU-derived

Received: September 8, 2013
Published: December 16, 2013

   dx.doi.org/10.1021/ic402280p | Inorg. Chem. 2014, 53, 327−335

Table 1. Crystal and Structure Refinement Data for 1−3[a]

	1	2	3
chem formula	$C_{72}H_{82}Cu_{20}N_{60}O_{47}S_4$	$C_{24}H_{31}Cu_6N_{12}O_{23.5}S_2$	$C_{12}H_{18}Cu_{3.5}N_6O_{13.5}S$
M_r	3939.02	1308.97	716.77
cryst size (mm)	0.13 × 0.11 × 0.10	0.15 × 0.14 × 0.13	0.18 × 0.17 × 0.16
cryst syst	triclinic	monoclinic	monoclinic
space group	$P\bar{1}$	$P2_1/c$	$P2_1/c$
a (Å)	16.1491(14)	10.4774(6)	7.4565(8)
b (Å)	20.6896(16)	21.9744(12)	17.0215(17)
c (Å)	20.7592(16)	19.6644(10)	17.1578(17)
α (deg)	113.4080(10)	90	90
β (deg)	123.605(7)	103.2840(10)	97.280(2)
γ (deg)	90.0770(10)	90	90
V (Å^3)	6290.2(9)	4406.3(4)	2160.1(4)
Z, D_c (g cm^{-3})	2, 2.080	4, 1.973	4, 2.204
$h/k/l$	−19, +15/−22, +24/−24, +21	−12, +12/−26, +25/−15, +23	−8, +8/−20, +19/−20, +14
F(000)	3908	2612	1430
μ (mm^{-1})	3.476	3.036	3.586
no of collected/unique rflns	32556/21989	22500/7757	10984/3807
R_{int}	0.0362	0.0373	0.0252
no. of data/restraints/params	21989/36/1828	7757/0/662	3807/48/350
R1[a]/wR2[b] ($I > 2\sigma(I)$)	0.0455/0.1026	0.0461/0.1118	0.0360/0.0828
R1/wR2 (all data)	0.0777/0.1111	0.0626/0.1210	0.0432/0.0868
max, min transmission	0.7226, 0.6608	0.6937, 0.6588	0.5977, 0.5645
GOF on F^2	1.010	1.039	1.042
$\Delta\rho_{max}$, $\Delta\rho_{min}$ (e Å^{-3})	1.233, − 0.644	0.827, − 0.961	0.756, − 0.881

[a] $R1 = \sum(||F_o| - |F_c||)/\sum|F_o|$. [b] $wR2 = [\sum w(|F_o|^2 - |F_c|^2)^2/\sum w(F_o^2)^2]^{1/2}$.

magnetic samples, a nanosized Cu^{II}_{30} metallamacrocycle-based pillared-layer framework (**1**), a 2-fold interpenetrated (3,6)-connected net with Cu^{II}_5 and Cu^{II}_1 motifs (**2**), and a (4,8)-connected architecture composed of centrosymmetric Cu^{II}_7 cores and four-branched sip^{3-} connectors (**3**), were hydrothermally generated by tuning the molar ratio of the metal to mixed ligands. Apparently, the various structures of **1**−**3** arise significantly from the variable intercluster connectivities and the slight expansion of the predesigned conformationally flexible Cu^{II}_5 SBUs. Magnetically, a field-dependent metamagnetic behavior from antiferromagnetic ordering to weak ferromagnetism is observed in **1**. Strong antiferromagnetic couplings in the ditopic ta^--extended Cu^{II}_5-containing ribbon of **2** give rise to a completely compensated moment and the separate Cu^{II}_1 core thus dominates the $S = {}^1/_2$ spin ground state. In contrast, strong antiferromagnetic interactions in the locally centrosymmetric Cu^{II}_7 cluster of **3** lead to an overall $S = {}^1/_2$ spin ground state. Insights gained from these investigations establish a novel strategy toward novel high-nuclearity cluster-based functional materials.

EXPERIMENTAL SECTION

Materials and Instruments. All initial chemicals were commercially purchased (Hta and NaH_2sip were from Acros and other analytical-grade reagents were from Tianjin Chemical Reagent Factory) and used as received without further purification. Elemental analyses for C, H, and N were carried out with a CE-440 (Leeman−Laboratories) analyzer. Fourier transform (FT) IR spectra (KBr pellets) were taken on an Avatar-370 (Nicolet) spectrometer in the range 4000−400 cm^{-1}. Thermogravimetric analysis (TGA) experiments were performed on a Shimadzu simultaneous DTG-60A compositional analysis instrument from room temperature to 800 °C under an N_2 atmosphere at a heating rate of 5 °C min^{-1}. Powder X-ray diffraction (PXRD) patterns were obtained with a Bruker D8 ADVANCE diffractometer at 40 kV and 40 mA for Cu Kα radiation (λ = 1.5406 Å), with a scan speed of 0.1 s/step and a step size of 0.01° in 2θ. The simulated PXRD pattern was calculated using single-crystal X-ray diffraction data and processed by the free Mercury v1.4 program provided by the Cambridge Crystallographic Data Center. Magnetic susceptibilities were acquired on a Quantum Design MPMS-XL-7 (SQUID) magnetometer with crystalline samples, in which the phase purity of the samples was determined by PXRD experiments. The diamagnetic corrections were calculated using Pascal's constants. In addition, an experimental correction for the sample holder was applied.

Synthesis of $\{[Cu_{20}(H_2O)_3(\mu_3\text{-}OH)_8(ta)_{20}(sip)_4]\cdot 8H_2O\}_n$ (1). A mixture of Hta (21.0 mg, 0.3 mmol), NaH_2sip (26.8 mg, 0.1 mmol), and $Cu(NO_3)_2\cdot 3H_2O$ (24.1 mg, 0.1 mmol) was dissolved in doubly deionized water (10.0 mL), and the initial pH value of the mixture was adjusted to 6.0 by triethylamine. The mixture was then transferred into a Parr Teflon-lined stainless steel vessel (23.0 mL) and heated to 160 °C for 72 h under autogenous pressure. After the mixture was cooled to room temperature at a rate of 1.6 °C h^{-1}, blue block-shaped crystals suitable for X-ray analysis were obtained directly, washed with water, and dried in air (yield 40.0% based on Cu^{II} salt). Anal. Calcd for $C_{72}H_{82}Cu_{20}N_{60}O_{47}S_4$: C, 21.95; H, 2.10; N, 21.34. Found: C, 21.96; H, 2.11; N, 21.34. IR (KBr, cm^{-1}): 3550 (s), 3471 (s), 3415 (s), 1639 (s), 1618 (s), 1434 (s), 1366 (s), 1189 (m), 1129 (m), 1039 (m), 979 (w), 840 (w), 799 (w), 777 (w), 621 (m), 482 (w), 410 (w).

Syntheses of $\{[Cu_6(H_2O)_6(\mu_3\text{-}OH)_2(ta)_4(sip)_2]\cdot 1.5H_2O\}_n$ (2) and $\{[Cu_7(H_2O)_2(\mu\text{-}OH)_2(\mu_3\text{-}OH)_2(ta)_4(sip)_2]\cdot 7H_2O\}_n$ (3). A mixture containing Hta (21.0 mg, 0.3 mmol), NaH_2sip (26.8 mg, 0.1 mmol), and $Cu(NO_3)_2\cdot 3H_2O$ (48.2 mg, 0.2 mmol) was dissolved in doubly deionized water (10.0 mL), and the initial pH value of the mixture was adjusted to ca. 6.0 by triethylamine. The mixture was then transferred into a Parr Teflon-lined stainless steel vessel (23.0 mL) and heated to 160 °C for 72 h under autogenous pressure. After the mixture was cooled to room temperature at a rate of 1.6 °C h^{-1}, blue hexagonal (for **2**) and rhombic block-shaped (for **3**) crystals suitable for X-ray analysis were obtained directly and separated manually, washed with water, and dried in air (yield 40.1% for **2** and 20.0% for **3** based on Cu^{II} salt). Anal. Calcd for $C_{24}H_{31}Cu_6N_{12}O_{23.5}S_2$ (**2**): C, 22.02; H, 2.39; N, 12.84. Found: C, 22.03; H, 2.40; N, 12.84. IR (KBr, cm^{-1}): 3550 (s), 3471 (br), 3415 (s), 1638 (s), 1618 (s), 1558 (s), 1436 (s), 1360

dx.doi.org/10.1021/ic402280p | Inorg. Chem. 2014, 53, 327−335

Table 2. Selected Geometric Parameters for the Cu^{II}_5 SBUs in 1−3

param	1				2	3
	1 with Cu1−Cu5	2 with Cu6−Cu10	3 with Cu11−Cu15	4 with Cu16−Cu20		
coordination polyhedron of the central Cu^{II} ion	planar square	square pyramid	square pyramid	square pyramid	square pyramid	octahedron
donor set of the central Cu^{II} ion	N_2O_2	N_2O_3	N_2O_3	N_2O_3	N_2O_3	N_2O_4
τ		0.60	0.21	0.57	0.21	
∠NCuN (deg)	142.5(2)	139.2(2)	160.4(2)	139.9(2)	167.0(2)	180.0(2)
∠OCuO (deg)	173.19(16)	175.21(16)	172.14(16)	173.98(17)	179.75(17)	179.999(1)
rel positions of two μ_3-OH^- groups	one side	one side	both sides	one side	both sides	both sides
dihedral angle of three Cu^{II} ion-generated triangular planes (deg)	31.5	33.5	23.1	32.3	3.9	0.0
r(O···triangular plane) (Å)	0.5282, 0.6597	0.5681, 0.5860	0.5120, 0.7068	0.5674, 0.5947	0.4834, 0.5709	0.5305, 0.5305
r(Cu···Cu within the triangular plane) (Å)	3.5127(3)	3.5238(3)	3.1354(2)	3.3981(2)	3.4621(2)	3.3151(3)
	3.3868(2)	3.3531(2)	3.3834(3)	3.3665(2)	3.2879(1)	3.3058(2)
	3.3984(2)	3.4401(2)	3.3255(2)	3.3527(2)	3.2912(1)	3.4437(3)
	3.4380(2)	3.4580(3)	3.4055(2)	3.4730(3)	3.2657(1)	
	3.3543(2)	3.3313(2)	3.3142(2)	3.4867(2)	3.3377(2)	
	3.3789(2)	3.3742(2)	3.4092(2)	3.4286(2)	3.3434(1)	

(s), 1210 (m), 1166 (m), 1131(m), 1112 (m), 1035 (m), 983 (w), 780 (w), 625 (m), 479 (w), 410 (w). Anal. Calcd for $C_{12}H_{18}Cu_{3.5}N_6O_{13.5}S$ (**3**): C, 20.11; H, 2.53; N, 11.72. Found: C, 20.12; H, 2.54; N, 11.74. IR (KBr, cm^{-1}): 3550 (s), 3471 (s), 3415 (s), 1637 (s), 1618 (s), 1560 (s), 1436 (s), 1363 (s), 1200 (m), 1127(m), 1044 (m), 986 (m), 726 (w), 624 (m), 482 (w), 410 (w).

X-ray Data Collection and Structure Determinations. Diffraction intensities for **1**−**3** were collected on a Bruker APEX-II QUAZAR diffractometer equipped with graphite-monochromated Mo Kα radiation with a radiation wavelength of 0.71073 Å by using the φ−ω scan technique at 296 K. There was no evidence of crystal decay during data collection. Semiempirical multiscan absorption corrections were applied by SADABS,[22] and the program SAINT[23] was used for integration of the diffraction profiles. The structures were solved by direct methods and refined with the full-matrix least-squares techniques using the SHELXS-97 and SHELXL-97 programs.[24] Anisotropic thermal parameters were assigned to all non-H atoms. The organic hydrogen atoms were geometrically generated. H atoms of the water molecules were located from difference maps and refined with isotropic temperature factors. Three solvent water molecules in **1** are disordered; therefore, the diffused electron densities resulting from these residual solvent molecules were removed from the data using the SQUEEZE routing of PLATON and refined further using the data generated.[25] Free water molecules (O45−O47 in **1**, O23W−O25W in **2**, and O13−O15 in **3**) are positionally disordered with the site occupancies refined to 0.75, 0.50, 0.25, 0.50, 0.50, 0.50, 0.70, 0.40, and 0.40, respectively. Three O donors from one sulfonate group of the sip^{3-} ligand (O5, O6, and O7) in **3** are positionally disordered between two symmetry-related positions with the site occupancies refined to 0.459 and 0.541. No hydrogen atom for the splitting water molecule was located because of the weak hydrogen-bonding interactions and the low site occupancy. The crystallographic data and selected geometric parameters are given in Tables 1 and 2. CCDC 955577, 955576, and 955578 for **1**−**3** contain supplementary crystallographic data for this paper. These data can be obtained, upon request, from the Director, Cambridge Crystallographic Data Centre, 12 Union Road, Cambridge CB21EZ, U.K.

RESULTS AND DISCUSSION

Syntheses and IR Spectra. Currently, it is more interesting and difficult to achieve various structures from the same reactant mixture. Herein, three predetermined Cu^{II}_5 cluster derived 3D frameworks were hydrothermally prepared by subtle tuning of the molar ratios of the metal to mixed ligands (1:3:1 for **1** and 2:3:1 for both **2** and **3**). In particular, the last two complexes with different appearance and mechanical hardness were generated together from a one-pot hydrothermal reaction. With the help of an optical microscope, bulky products of **2** and **3** can be clearly distinguished with the naked eye and were separated manually and carefully for the subsequent structural and magnetic measurements. Triethylamine was used to control the pH value of the reaction medium. Additionally, all of the products are air-stable and are almost insoluble in water and common organic solvents due to their polymeric structures.

In the IR spectra of **1**−**3**, three strong bands centered at 3415 cm^{-1} for the O−H stretching vibration and an absence of a strong absorption at ca. 1700 cm^{-1} respectively confirm the presence of a water molecule and the full deprotonation of the H_2sip^- anion. As a result of the splitting of the strong asymmetric and symmetric stretch vibrations for the carboxylate and sulfonate moieties of the sip^{3-} ligand, slight differences are clearly observed between 1639 and 1360 cm^{-1} (1338 ± 1, 1618, and 1435 ± 1, 1363 ± 3 cm^{-1} for **1**−**3** and an additional signal at 1559 ± 1 cm^{-1} for both **2** and **3**) as well as between 1200 and 1035 cm^{-1}. Their distinct separations and splitting may suggest the variable binding modes (Figure S1, Supporting Information),[26] which are in good agreement with the single-crystal X-ray diffraction data.

Crystal Structure of $\{[Cu_{20}(H_2O)_3(\mu_3\text{-}OH)_8(ta)_{20}(sip)_4]\cdot 8H_2O\}_n$ (1). Complex **1** is an open pillared-layer framework constructed from nanosized Cu^{II}_{30} metallamacrocycle-based sublayers and directional sip^{3-} pillars. The asymmetric unit of **1** contains four crystallographically independent $[Cu_5(\mu_3\text{-}OH)_2(ta)_4]^{4+}$ SBUs with or without a coordinated water molecule, two pairs of μ_3-ta^- linkers that connect three pairs of Cu^{II}_5 subunits into a Cu^{II}_{30} metallamacrocycle, four fully deprotonated sip^{3-} spacers, and some lattice water molecules. As shown in Figure 1a, all the Cu^{II}_5 cores in **1** are consistently composed of five crystallographically independent Cu^{II} ions with different coordination polyhedra (distorted square-planar, square-pyramidal, and/or octahedral geometries; see Figure S2 and Table S1 in the Supporting Information) completed by N_xO_y (x = 2−4; y = 1−3) donor sets, two asymmetric μ_3-OH^- groups that respectively aggregate three unique Cu^{II} ions into two corner-sharing triangles, and four μ_3-ta^- anions. Notably, the conformations of these Cu^{II}_5 SBUs in **1** are flexible and

dx.doi.org/10.1021/ic402280p | Inorg. Chem. 2014, 53, 327−335

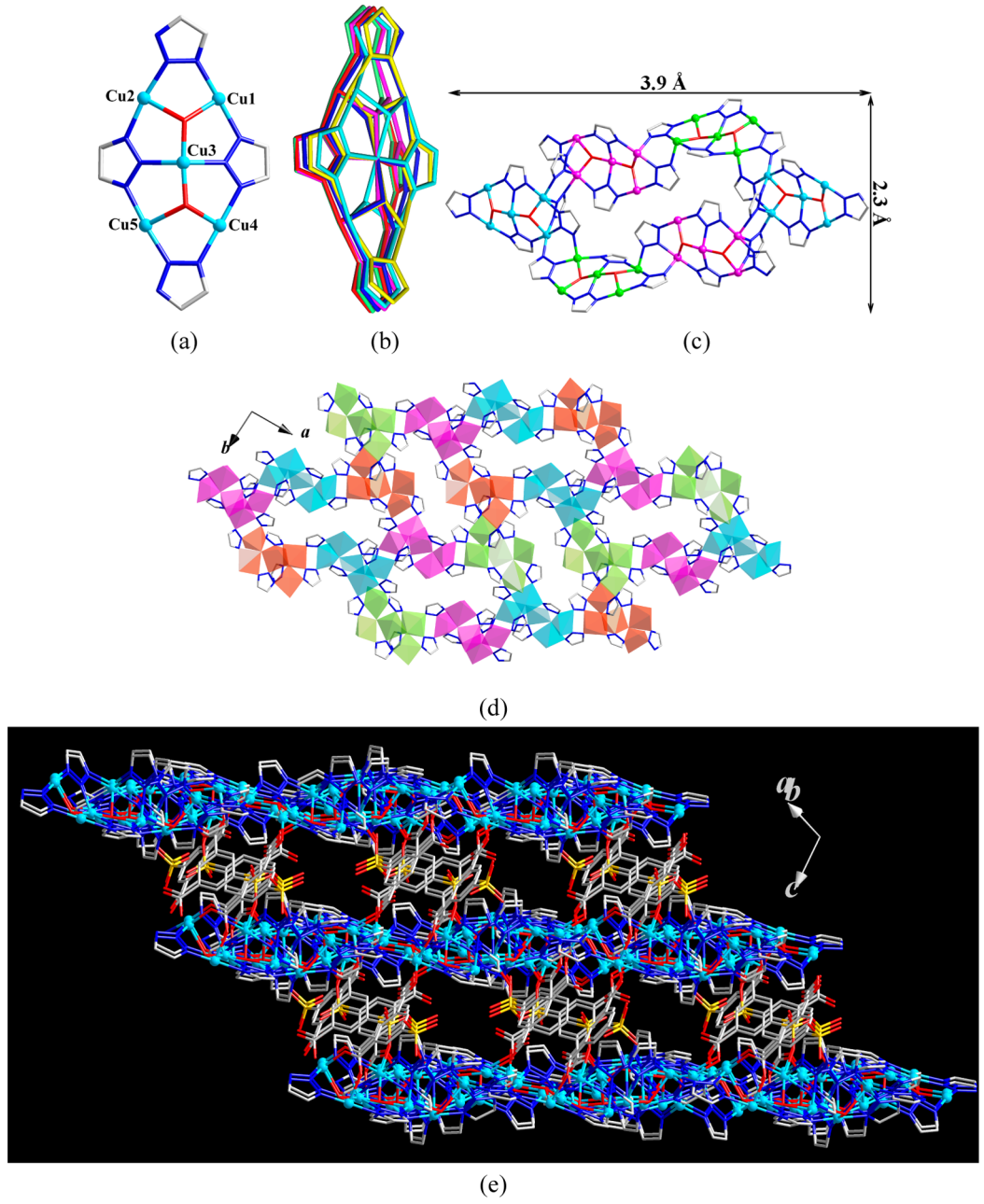

Figure 1. (a) Local $[Cu_5(\mu_3\text{-}OH)_2(ta)_4]^{4+}$ cluster in **1**. (b) Superposition diagram of the local Cu^{II}_5 SBUs in **1** (red, green, blue, and purple), **2** (yellow), and **3** (cyan). (c) Nanosized Cu^{II}_{30} metallamacrocycle generated from three pairs of equivalent Cu^{II}_5 cores and two μ_3-ta^- connectors. (d) Cu^{II}_{30} metallamacrocycle-based sublayer of **1**. (e) Pillared-layer framework of **1**.

differ slightly from each other (Figure 1b). Geometrically, the conformation of the Cu^{II}_5 SBU is more significantly influenced by the $\angle NCu_{central}N$ angle involved in the central, distorted-square-planar and/or square-pyramidal Cu^{II} ion, rather than the $\angle OCu_{central}O$ angle (see Table 2). The larger the $\angle NCu_{central}N$ angle, the smaller the dihedral angle of three Cu^{II} ion generated triangular planes (Table 2). Thus, the conformational flexibility of the Cu^{II}_5 precursors is considered as one of the important preconditions governing the self-assembly process.

As shown in Figure 1c, three unique Cu^{II}_5 cores in **1** are aggregated together into an arc-shaped fragment by the N3 donor of the outer ta^- ligand coordinating to the Cu^{II} ion from the neighboring Cu^{II}_5 SBU. Two centrosymmetric fragments are further connected end to end by an additional pair of unique μ_3-ta^- linkers, generating an elliptical Cu^{II}_{30} metallamacrocycle of the size 3.9 × 2.3 Å (Figure 1c). As mentioned above, complex **1** contains four unique Cu^{II}_5 cores; therefore, two crystallographically different Cu^{II}_{30} metallamacrocycles are generated with comparable sizes. To the best of our knowledge, only a few examples with Cu^{II}_8, Cu^{II}_{12}, Cu^{II}_{20}, Co^{II}_{24}, and Cu^{II}_{30} metallamacrocycles have been reported to date by using triazolate-family ligands and different template molecules or counterions.[13,27,28]

As can be seen from Figure 1d, the nanosized Cu^{II}_{30} metallamacrocycles are further fused together with the remaining N3 donor binding the Cu^{II} ions from the other Cu^{II}_{30} unit, generating an approximately coplanar sublayer of **1**. Apparently, all of the Cu^{II} ions within the sublayer are arranged in various vertex-sharing triangles (Figure S3, Supporting Information), which could possibly induce frustrated magnetic

dx.doi.org/10.1021/ic402280p | Inorg. Chem. 2014, 53, 327−335

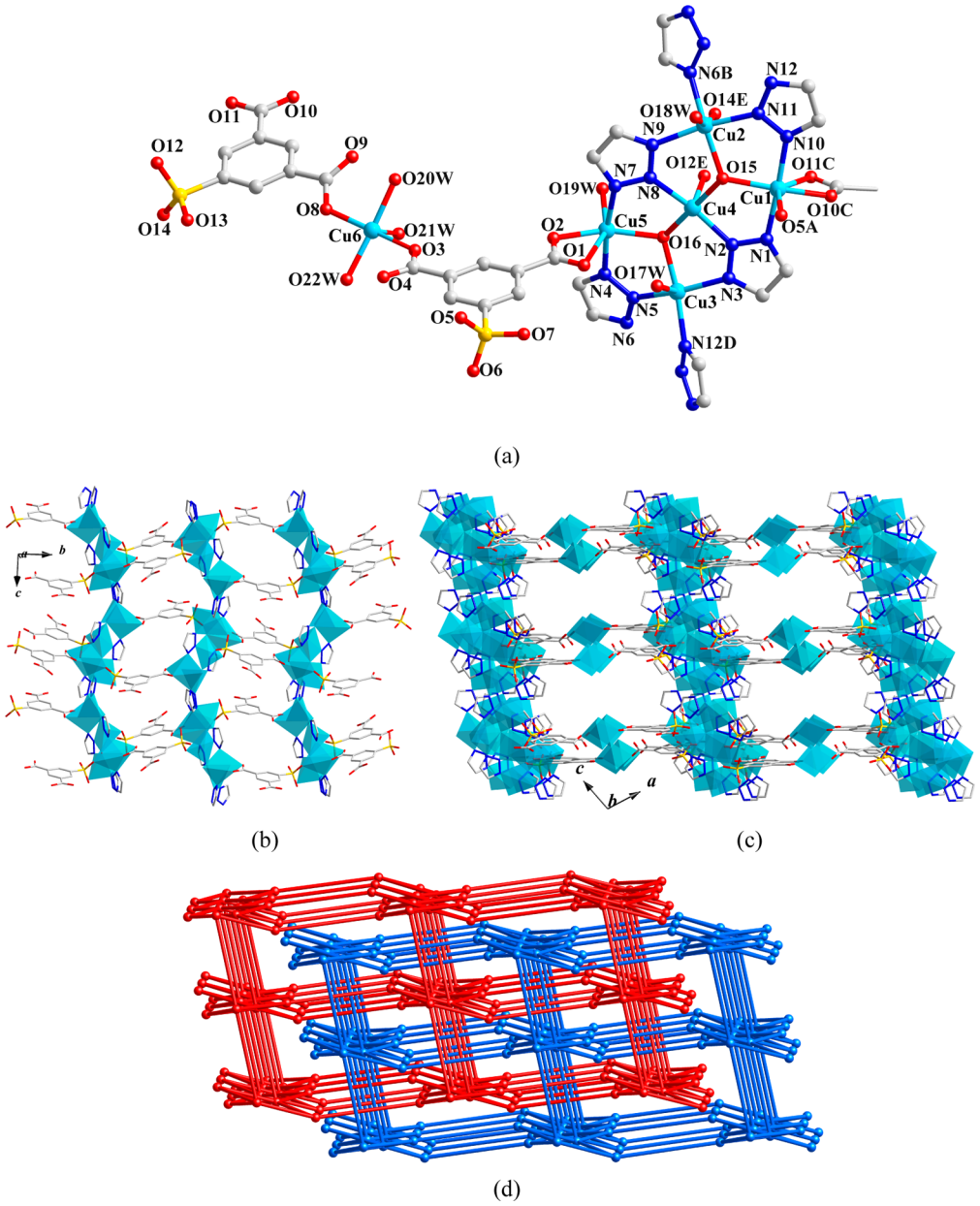

Figure 2. (a) Local coordination environment of Cu^{II} atoms in **2** (H atoms and part of phenyl moiety of sip^{3-} are omitted for clarity). Symmetry codes: (A) $2-x, 1-y, 1-z$; (B) $x-0.5, 0.5-y, z-0.5$; (C) $x+1.5, 0.5-y, z-0.5$; (D) $x+0.5, 0.5-y, z+0.5$; (E) $0.5-x, y-0.5, 1.5-z$. (b) 2D layer of **2** with Cu^{II}_5 SBUs extended by ta^- and sip^{3-} connectors. (c) 3D framework of **2** with Cu^{II}_1 cores bridging the adjacent layers. (d) Twofold (color separated in blue and red) interpenetrated framework of **2**.

behavior.[29] The adjacent sublayers of **1** are well separated by the sip^{3-} spacers, giving rise to an open pillared-layer framework (Figure 1e). The interlayer metallic separation spanned by the rigid sip^{3-} linker is ca. 10 Å, suggesting potentially weak interlayer magnetic interactions.[30]

Crystal Structure of $\{[Cu_6(H_2O)_6(\mu_3\text{-}OH)_2(ta)_4(sip)_2]\cdot 1.5H_2O\}_n$ (2). Complex **2** assumes a 2-fold interpenetrating (3,6)-connected topological net, in which approximately coplanar Cu^{II}_5 and square-pyramidal Cu^{II}_1 cores are periodically interlinked by trifurcate sip^{3-} and ditopic μ_3-ta^- heterolinkers. The asymmetric unit of **2** contains one predesigned Cu^{II}_5 SBU with three extra aqua ligands, one distorted-square-pyramidal Cu6 ion with Addison parameter $\tau = 0.05$ (the Addison parameter is defined as an index of trigonality),[31] two triply deprotonated sip^{3-} connectors in two different binding modes (Figure S1, Supporting Information), and one and a half lattice water molecules.

The coplanarity of the Cu^{II} ions in the Cu^{II}_5 SBU of **2** is greatly improved in comparison with those in **1**. The dihedral angle of the two Cu^{II}-containing triangular planes is only 3.898(19)°, resulting from the slight distortion of the square-pyramidal Cu4 ($\tau = 0.21$) and Cu3 ($\tau = 0.18$) as well as the octahedral Cu1, Cu2, and Cu5 ions (Figure 2a and Table S2 in the Supporting Information). Moreover, two independent μ_3-OH^- groups are situated on the opposite side of the corner-sharing triangular planes, which also essentially decreases the spatial steric hindrance and benefits the coplanar alignment of the Cu^{II} ions. The intermetallic distances within the Cu^{II}_5 cluster are between 3.2657(1) and 3.4621(2) Å (Table 2), favorable for the magnetic interactions in **2**.

dx.doi.org/10.1021/ic402280p | Inorg. Chem. 2014, 53, 327−335

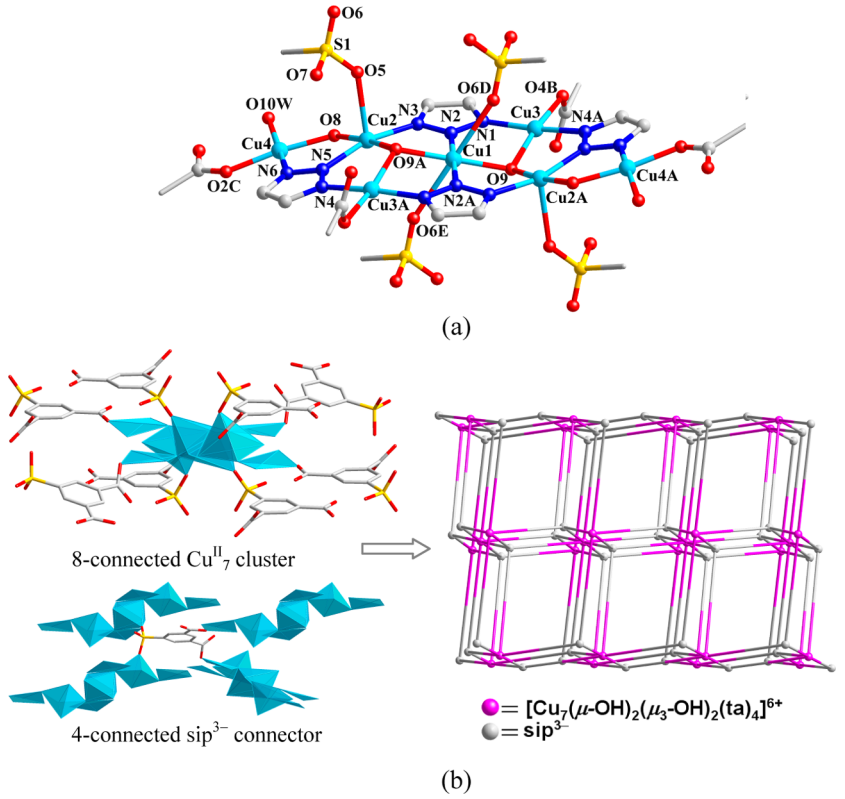

Figure 3. (a) Heptanuclear subunit of **3** (H atoms and part of the phenyl moiety of sip^{3-} are omitted for clarity). Symmetry codes: (A) $2-x, 2-y, 2-z$; (B) $1-x, y+0.5, 1.5-z$; (C) $1-x, 1-y, 2-z$; (D) $1-x, 2-y, 2-z$; (E) $1+x, y, z$. (b) Connections of Cu$^{II}_7$ cluster and sip^{3-} ligand (left) and the (4,8)-connected topological net of **3** (right).

Each Cu$^{II}_5$ cluster in **2** is periodically expanded by two different kinds of connectors (pairs of ta$^-$ and sip^{3-} ligands), leading to an approximately coplanar layer stacked in the crystallographic *bc* plane (Figure 2b). The intercluster distance (3.6431(2) Å) separated by the ditopic μ_3-ta$^-$ connector is considerably shorter by 5.4 Å in comparison to that by the sip^{3-} anion (ca. 10.0 Å), although it is comparable with those within the Cu$^{II}_5$ core. Thus, the antiferromagnetic superexchange is also expected in the locally μ_3-ta$^-$ extended 1D ribbon. The neighboring layers of **2** are further joined together by the coordination of the other monodentate carboxylate group of the sip^{3-} ligand with the square-pyramidal Cu6 ion, leading to a novel 3D coordination structure of **2**, as illustrated in Figure 2c.

In the overall 3D structure of **2**, each [Cu$_5$(μ_3-OH)$_2$(ta)$_4$]$^{4+}$ cluster is surrounded by four neighbors through four sip^{3-} and two pairs of μ_3-ta$^-$ linkers and can be considered as a four-connected node (Figure S4, Supporting Information). Despite adopting two different binding modes, both of the unique sip^{3-} anions in **2** can be considered as 3-connected nodes (Figure S4), because they both aggregate two Cu$^{II}_5$ cores and one square-pyramidal Cu6 ion together. In contrast, the μ_3-ta$^-$ ligands that propagate the Cu$^{II}_5$ SBUs into a 1D ribbon and the Cu6 square pyramid can serve as two different kinds of linkers. Thus, **2** belongs to a rare binodal (3,6)-connected *sqc*27 topological net (Figure 2d) with the Schläfli symbol of $(4\cdot6^2)_2(4^2\cdot6^{10}\cdot8^3)$ obtained by TOPOS.[32] More interestingly, two identical 3D nets of **2** are interlocked with each other, leading to a 2-fold interpenetrated 3D → 3D structure (Figure 2d). Notably, the interpenetrated framework has been scarcely observed in the polynuclear metal cluster-based coordination polymers so far, because the multiple linkers around the polynuclear metal cluster can produce severe steric repulsions and prevent the formation of interpenetration.

Crystal Structure of {[Cu$_7$(H$_2$O)$_2$(μ-OH)$_2$(μ$_3$-OH)$_2$(ta)$_4$(sip)$_2$]·7H$_2$O}$_n$ (3). Complex **3** crystallizes in the monoclinic $P2_1/c$ space group, exhibiting a (4,8)-connected net with centrosymmetric Cu$^{II}_7$ clusters extended by four-branched sip^{3-} linkers. The fundamental unit of **3** contains a centrosymmetric [Cu$_7$(H$_2$O)$_2$(μ-OH)$_2$(μ_3-OH)$_2$(ta)$_4$]$^{6+}$ subunit, two crystallographically equivalent sip^{3-} linkers, and some disordered lattice water molecules. The heptanuclear subunit in **3** can be considered as a slight expansion of the predetermined [Cu$_5$(μ_3-OH)$_2$(ta)$_4$]$^{4+}$ precursor, in which two additionally centrosymmetric Cu4 and Cu4A ions with distorted-square-planar coordination spheres are incorporated into the predesigned Cu$^{II}_5$ cluster by two bridging μ-OH$^-$ groups and two outer ta$^-$ ligands (Figure 3a). Moreover, the heterocyclic structure involving the newly generated Cu4 ion is five-membered, which is thermodynamically stable and structurally favorable for the expansion of the Cu$^{II}_5$ core. The intermetallic distances within the Cu$^{II}_7$ cluster are slightly varied in comparison with those in **1** and **2** (Table 2), in which the nonbinding Cu2···Cu4 distance is 3.3644(3) Å. Notably, the predesigned Cu$^{II}_5$ SBU in **3** is centrosymmetric with the centered Cu1 ion in axially elongated octahedral N_2O_4 surroundings (Figure 3a, Table S3 and Figure S5 in the Supporting Information), which is much different from the nonsymmetric subunits in **1** and **2** with distorted tetra- and pentacoordinated metal spheres. Apparently, the five metal ions are strictly coplanar with two μ_3-OH$^-$ groups locating on the opposite side of the planes, similar to one (formed by Cu11–Cu15) of the Cu$^{II}_5$ cores in **1**.

dx.doi.org/10.1021/ic402280p | *Inorg. Chem.* 2014, 53, 327–335

As shown in Figure 3b, each centrosymmetric Cu^{II}_7 cluster in **3** is repeatedly surrounded by eight sip^{3-} ligands through the coordination of Cu^{II} ions with sulfonate and carboxylate groups of the sip^{3-} ligand and thus can be topologically served as an 8-connected node. In contrast, each sip^{3-} connector aggregates four separate Cu^{II}_7 clusters and acts as a 4-connected node. The 4- and 8-connected nodes are repeatedly arranged to generate a (4,8)-connected 3D framework of **3** with the Schläfli symbol of $(4^4{\cdot}6^2)_2(4^{10}{\cdot}6^{14}{\cdot}8^4)^{32}$ (Figure 3b). The nearest intercluster $Cu^{II}{\cdots}Cu^{II}$ distance spanned by the short sulfonate group of the sip^{3-} linker is 6.675 Å, insufficient for intercluster magnetic transfer. Therefore, the local Cu^{II}_7 cluster is expected to govern the magnetic interactions of **3**.

PXRD Patterns and Thermogravimetric Analyses. TGA experiments were conducted between room temperature and 800 °C in order to explore the compositional thermal stability of **1**−**3** (Figure S6, Supporting Information). As a result, complex **1** displayed three distinct weight-loss steps. The first one that began at 68 °C and ended at 103 °C should be ascribed to the release of the coordinated and lattice water molecules (obsd 5.0%, calcd 4.7%). The combustion of the mixed ta^- and sip^{3-} ligands as well as the μ_3-OH^- group of **1** were subsequently observed between 303 and 484 °C (obsd 49.6%, calcd 51.5%) as well as between 596 and 710 °C (obsd 4.5%, calcd 3.5%). The final residue of **1** above 710 °C was CuO (obsd 40.7%, calcd 40.3%). In contrast, the last two samples exhibited two separate weight-loss processes with the first one starting at room temperature and finishing at 174 °C for the removal of lattice and/or coordinated water molecules (obsd 9.7%, calcd 10.3% for **2** and obsd 9.7%, calcd 8.8% for **3**). Once the temperature was higher than 300 °C, the skeletal collapses of **2** and **3** occurred, which were completely finished at the highest temperature measured. The structural consistency and phase purity of the bulk products of **1**−**3** were also evidenced by comparisons of the experimental and computer-simulated PXRD patterns (Figure S7, Supporting Information). Notably, the slight difference in the experimental and theoretical powder diffraction patterns for **2** was probably due to the crystallographically preferred orientation of the grains, a reduction in crystallite size, and an increase in lattice strain.

Magnetic Properties. Variable-temperature (2−300 K) magnetic susceptibilities of **1**−**3** were measured on crystalline samples under an applied direct-current (dc) field of 2.0 kOe. As shown in Figure 4a, the $\chi_M T$ product per Cu^{II}_{20} subunit of **1** is 6.48 cm^3 K mol^{-1} at 300 K, much less than the predicted value (7.50 cm^3 K mol^{-1}) for 20 magnetically isolated Cu^{II} ions with $S = {}^1/_2$ and $g = 2.0$. Upon cooling, the $\chi_M T$ value decreases rapidly and reaches a minimum value of 0.09 cm^3 K mol^{-1} at 2.0 K. The appearance of a sharp peak at 4.5 K in the χ_M vs T curve implies a weak antiferromagnetic ordering of **1** (Figure S8, Supporting Information), which structurally arises from the intralayer antiferromagnetic couplings mediated by the μ_3-ta^- bridges. The Néel temperature (T_N) is 3.5 K, obtained from the peak in $d(\chi_M T)/dT$ (Figure S8). Furthermore, the curve of $\chi_M{}^{-1}$ vs T obeys the Curie−Weiss law well above 100 K with curie constant $C = 9.98$ cm^3 K mol^{-1} and Weiss constant $\Theta = -199.1$ K (Figure 4a, insert), indicating that strong antiferromagnetic interactions occur in the nearest neighbors of **1** mediated by μ_3-ta^- and μ_3-OH^- heterobridges. On the other hand, due to the corner-sharing triangular arrangement of the spin carriers in the antiferromagnetically coupled Cu^{II}_{30}-containing sublayer, strong spin frustration is observed in **1**, in which the frustration extent defined by the ratio of the Weiss constant to the ordering temperature ($f = |\Theta|/T_N$) is ca. 19.9.

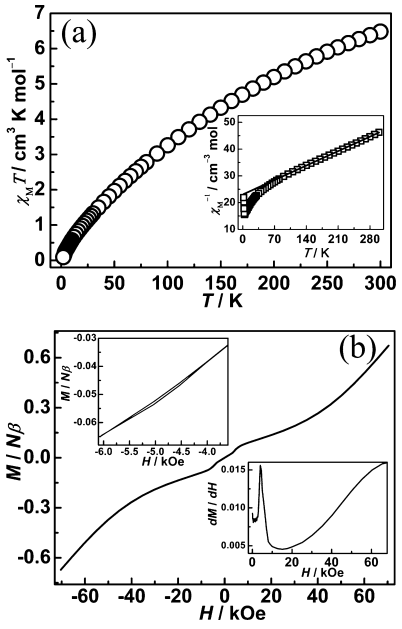

Figure 4. (a) Temperature dependence of $\chi_M T$ for **1**. Inset: plot of $\chi_M{}^{-1}$ vs T, with the solid lines corresponding to the best fit to the Curie−Weiss law. (b) M vs H curve for **1** at 2.0 K. Inset: the magnetic hysteresis loop of **1** at 2.0 K and plot of dM/dH vs H.

The magnetization curve for **1** at 2.0 K shows a field-dependent sigmoid characteristic of metamagnetism (Figure 4b). The magnetization linearly increases with the enhanced external magnetic field below 3.0 kOe. Then, a slightly steep increase is observed between 3.0 and 6.8 kOe. Upon a further increase in the field, a serious deviation from the linear relationship of the magnetization is followed due to the reorientation of the spins. The magnetization of **1** at 70 kOe (0.67 $N\beta$) is below the value even for one Cu^{II} ion (1.0 $N\beta$), consistent with weak ferromagnetism originated from the magnetic competitions within the frustrated Cu^{II}_{30} metallamacrocycle-containing sublayer of **1**. The critical field for the metamagnetic transition is about 4.0 kOe, calculated by the maximum dM/dH value. Additionally, a slight hysteresis loop corresponding to the spontaneous magnetization is observed (Figure 4b, inset), which further confirms the metamagnetic transition of **1**.

For the last two complexes, the plots of $\chi_M{}^{-1}$ vs T above 130 K obey the Curie−Weiss law well with $C = 2.52$ cm^3 K mol^{-1} and $\Theta = -208$ K for **2** and $C = 2.81$ cm^3 K mol^{-1} and $\Theta = -182$ K for **3** (Figure 5a inset), suggesting that comparable antiferromagnetic interactions exist in the nearest spin carriers despite their different Cu^{II}_5 + Cu^{II}_1 and Cu^{II}_7 motifs. Careful comparisons of $\chi_M T$ vs T curves reveal only slight differences. The $\chi_M T$ value at 300 K is 1.61 cm^3 K mol^{-1} per Cu^{II}_5 + Cu^{II}_1 of **2**, while it is 1.70 cm^3 K mol^{-1} per Cu^{II}_7 subunit of **3**. Upon cooling, the $\chi_M T$ of **2** drops continuously and reaches a minimum of 0.42 cm^3 K mol^{-1} at 2.0 K. For **3**, $\chi_M T$ quickly drops to 0.44 cm^3 K mol^{-1} at 4.0 K arising from the intracluster antiferromagnetic interactions and then slowly decreases to the minimum value of 0.41 cm^3 K mol^{-1} at 2.0 K due to the weak intercluster antiferromagnetic interactions mediated by the sip^{3-} connectors. The minimum $\chi_M T$ values at 2.0 K strongly suggest an overall $S = {}^1/_2$ spin ground state is populated at low

dx.doi.org/10.1021/ic402280p | Inorg. Chem. 2014, 53, 327−335

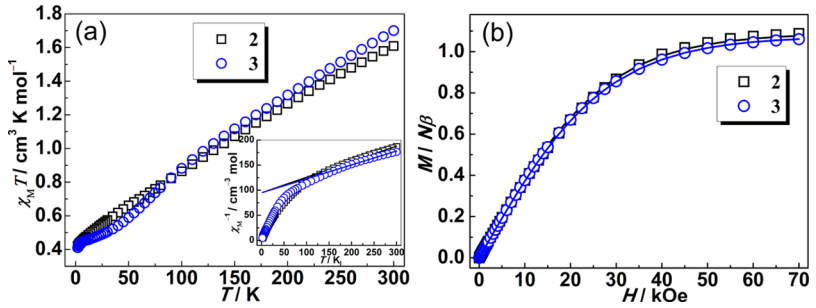

Figure 5. (a) Temperature dependence of $\chi_M T$ for **2** and **3**. Inset: plot of χ_M^{-1} vs T (the solid lines correspond to the best fit by the Curie−Weiss law). (b) M vs H curves for **2** and **3** at 2.0 K. The solid lines correspond to the best fit to the Brillouin function.

temperature for both **2** and **3**, which can be further confirmed by the magnetizations (1.09 and 1.06 $N\beta$) at 70 kOe (Figure 5b). Additionally, both of the $M-H$ curves obey the Brillouin function well with $S = {}^1/_2$, $g = 2.17$, and $R = \sum[(\chi_M T)_{obsd} - (\chi_M T)_{calcd}]^2/\sum[(\chi_M T)_{obsd}]^2 = 2.4 \times 10^{-3}$ for **2**, and $S = 1/2$, $g = 2.15$, and $R = 4.2 \times 10^{-4}$ for **3** (Figure 5b), meaning that weak antiferromagnetic interactions exist between the overall magnetic subunits with $S = {}^1/_2$. From a viewpoint of the magneto-structural relationship, the magnetic couplings in **2** are essentially dominated by pairs of ditopic ta$^-$-bridged 1D ribbons due to the long nonbonding Cu^{II}···Cu^{II} distance separated by the sip^{3-} anions. All of the Cu^{II} ions in the ribbon are antiferromagnetically coupled by the μ_3-OH$^-$ and −NN− moieties of μ_3-ta$^-$ mediators; the magnetization within the ribbon is thus completely canceled out. Therefore, the remaining Cu6 ion serves as a paramagnetic component and essentially contributes to the $S = {}^1/_2$ spin ground state of **2**. However, for **3**, the $S = {}^1/_2$ spin ground state obviously results from the uncompensated magnetic moment in the centrosymmetric Cu$^{II}_7$ cluster. Apparently, although both **2** and **3** can be populated to an $S = {}^1/_2$ spin ground state at low temperature, their superexchange pathways are different.

CONCLUSION

In summary, we have demonstrated a new SBU-involved self-assembly strategy and further validated the method in the ternary Cu^{II}−triazolate−sulfoisophthalate system. Controllable hydrothermal reactions of the system respectively afforded an open pillared-layer framework consisting of nanosized Cu$^{II}_{30}$ metallamacrocycles, a (3,6)-connected 2-fold interpenetrating net with Cu$^{II}_5$ and Cu$^{II}_1$ subunits, and a (4,8)-connected architecture possessing centrosymmetric Cu$^{II}_7$ clusters. Structurally, the predesigned, conformationally flexible Cu$^{II}_5$ SBUs become the most important factors for the self-assembly process, which are periodically aggregated by the polytopic sip^{3-} connectors for the resulting structural diversity. More importantly, these interesting motifs further induce different metamagnetic and antiferromagnetic behaviors. Therefore, the self-assembly strategy from the predetermined SBU opens up a new window for the novel functional materials.

ASSOCIATED CONTENT

Supporting Information

Figures, tables, and CIF files giving binding modes of the rigid sip^{3-} ligand, selected bond lengths and angles, TG curves, PXRD patterns, additional structural figures, X-ray crystallographic data for **1**−**3**, and plots of χ_M and $d(\chi_M T)/dT$ vs T for **1**. This material is available free of charge via the Internet at http://pubs.acs.org.

AUTHOR INFORMATION

Corresponding Author

*E-mail: encui_yang@163.com (E.-C.Y.); xiaojun_zhao15@163.com (X.-J.Z.). Fax: +86-22-23766556.

Notes

The authors declare no competing financial interest.

ACKNOWLEDGMENTS

This present work was financially supported by the National Natural Science Foundation of China (Grants 21171129 and 21173157), the 973 Program (2014CB845601), the Program for Innovative Research Team in University of Tianjin, and Tianjin Municipal Education Commission (2012ZD02), which are gratefully acknowledged.

REFERENCES

(1) Bai, Y.-L.; Tao, J.; Huang, R.-B.; Zheng, L.-S. *Angew. Chem., Int. Ed.* **2008**, *47*, 5344−5347.

(2) Xiao, J.; Liu, B.-Y.; Wei, G.; Huang, X.-C. *Inorg. Chem.* **2011**, *50*, 11032−11038.

(3) (a) Laye, R. H.; Wei, Q.; Mason, P. V.; Shanmugam, M.; Teat, S. J.; Brechin, E. K.; Collison, D.; McInnes, E. J. L. *J. Am. Chem. Soc.* **2006**, *128*, 9020−9021. (b) Low, D. M.; Jones, L. F.; Bell, A.; Brechin, E. K.; Mallah, T.; Riviére, E.; Teat, S. J.; McInnes, E. J. L. *Angew. Chem., Int. Ed.* **2003**, *42*, 3781−3784.

(4) Shao, K.-Z.; Zhao, Y.-H.; Wang, X.-L.; Lan, Y.-Q.; Wang, D.-J.; Su, Z.-M.; Wang, R.-S. *Inorg. Chem.* **2009**, *48*, 10−12.

(5) Shaw, R.; Laye, R. H.; Jones, L. F.; Low, D. M.; Talbot-Eeckelaers, C.; Wei, Q.; Milios, C. J.; Teat, S.; Helliwell, M.; Evangelisti, M.; Affronte, M.; Collison, D.; Brechin, E. K.; Mclnnes, E. J. L. *Inorg. Chem.* **2007**, *46*, 4968−4978.

(6) (a) Ouellette, W.; Liu, H.-X.; O'Connor, C. J.; Zubieta, J. *Inorg. Chem.* **2009**, *48*, 4655−4657. (b) Ouellette, W.; Yu, M. H.; O'Connor, C. J.; Hagrman, D.; Zubieta, J. *Angew. Chem., Int. Ed.* **2006**, *45*, 3497−3500. (c) Ouellette, W.; Galán-Mascarós, J. R.; Dunbar, K. R.; Zubieta, J. *Inorg. Chem.* **2006**, *45*, 1909−1911.

(7) Wu, T.; Li, M.; Li, D.; Huang, X.-C. *Cryst. Growth Des.* **2008**, *8*, 568−574.

(8) Wang, X.-L.; Qin, C.; Lan, Y.-Q.; Shao, K.-Z.; Su, Z.-M; Wang, E.-B. *Chem. Commun.* **2009**, 410−412.

(9) (a) Yang, E.-C.; Ding, B.; Liu, Z.-Y.; Yang, Y.-L.; Zhao, X.-J. *Cryst. Growth Des.* **2012**, *12*, 1185−1192. (b) Yang, E.-C.; Yang, Y.-L.; Liu, Z.-Y.; Liu, K.-S.; Wu, X.-Y.; Zhao, X.-J. *CrystEngComm* **2011**, *13*, 2667−2673. (c) Yang, E.-C.; Liu, Z.-Y.; Shi, X.-J.; Liang, Q.-Q.; Zhao, X.-J. *Inorg. Chem.* **2010**, *49*, 7969−7975. (d) Yang, E.-C.; Zhang, C.-H.; Liu, Z.-Y.; Zhang, N.; Zhao, L.-N.; Zhao, X.-J. *Polyhedron* **2012**, *40*, 65−67. (e) Yang, E.-C.; Liu, Z.-Y.; Zhang, C.-H.; Yang, Y.-L.; Zhao, X.-J. *Dalton Trans.* **2013**, *42*, 1581−1590. (f) Yang, E.-C.; Liu, Z.-Y.; Wu, X.-Y.; Chang, H.; Wang, E.-C.; Zhao, X.-J. *Dalton Trans.* **2011**, *40*, 10082−10089.

(10) Liu, Y.-Y.; Grzywa, M.; Tonigold, M.; Sastre, G.; Schüttrigkeit, T.; Leeson, N. S.; Volkmer, D. *Dalton Trans.* **2011**, *40*, 5926−5938.
(11) Zhou, X.-H.; Peng, Y.-H.; Du, X.-D.; Zuo, J.-L.; You, X.-Z. *CrystEngComm* **2011**, *11*, 1964−1970.
(12) Biswas, S.; Tonigold, M.; Speldrich, M.; Kögerler, P.; Weil, M.; Volkmer, D. *Inorg. Chem.* **2010**, *49*, 7424−7434.
(13) Ruan, C.-Z.; Wen, R.; Liang, M.-X.; Kong, X.-J.; Ren, Y.-P.; Long, L.-S.; Huang, R.-B.; Zheng, L.-S. *Inorg. Chem.* **2012**, *51*, 7587−7591.
(14) Zhong, D.-C.; Deng, J.-H.; Luo, X.-Z.; Liu, X.-J.; Zhong, J.-L; Wang, K.-J.; Lu, T.-B. *Cryst. Growth Des.* **2012**, *12*, 1992−1998.
(15) Wang, X.-L.; Qin, C.; Wu, S.-X.; Shao, K.-Z.; Lan, Y.-Q.; Wang, S.; Zhu, D.-X.; Su, Z.-M.; Wang, E.-B. *Angew. Chem., Int. Ed.* **2009**, *48*, 5291−5295.
(16) Yang, E.-C.; Zhao, H.-K.; Ding, B.; Wang, X.-G.; Zhao, X.-J. *Cryst. Growth Des.* **2007**, *7*, 2009−2015.
(17) Wang, X.-L.; Wang, Y.-F.; Liu, J.-C.; Tian, A.-X.; Zhang, G.-W.; Lin, H.-Y. *Dalton Trans.* **2011**, *40*, 9299−9305.
(18) Park, H.; Moureau, D. M.; Parise, J. B. *Chem. Mater.* **2006**, *18*, 525−531.
(19) Joosten, A.; Trolez, Y.; Collin, J.-P.; Heitz, V.; Sauvage, J.-P. *J. Am. Chem. Soc.* **2012**, *134*, 1802−1809.
(20) Zhang, J.-P.; Lin, Y.-Y.; Huang, X.-C.; Chen, X.-M. *J. Am. Chem. Soc.* **2005**, *127*, 5495−5506.
(21) Clearfield, A.; Demadis, K. *Metal Phosphonate Chemistry*; RSC: Cambridge, U.K., 2012.
(22) Sheldrick, G. M. *SADABS*; University of Göttingen, Göttingen, Germany, 1996.
(23) *SAINT Software Reference Manual*, Bruker AXS: Madison, WI, 1998.
(24) (a) Sheldrick, G. M. *SHELXL-97, Program for X-ray Crystal Structure Refinement*; University of Göttingen, Göttingen, Germany, 1997. (b) Sheldrick, G. M. *SHELXS-97, Program for X-ray Crystal Structure Solution*; University of Göttingen, Göttingen, Germany, 1997.
(25) Spek, A. L. *J. Appl. Crystallogr.* **2003**, *36*, 7−13.
(26) Nakamoto, K. *Infrared and Roman Spectra of Inorganic and Coordination Compounds*; Wiley: New York, 1986.
(27) Xu, Z.-Q.; Wang, Q.; Li, H.-J.; Meng, W.; Han, Y.; Hou, H.-W.; Fan, Y.-T. *Chem. Commun.* **2012**, *48*, 5736−5738.
(28) Han, S.-D.; Song, W.-C.; Zhao, J.-P.; Yang, Q.; Liu, S.-J; Li, Y.; Bu, X.-H. *Chem. Commun.* **2013**, *49*, 871−873.
(29) (a) Shores, M. P.; Nytko, E. A.; Bartlett, B. M.; Nocera, D. G. *J. Am. Chem. Soc.* **2005**, *127*, 13462−13463. (b) Nytko, E. A.; Helton, J. S.; Müller, P.; Nocera, D. G. *J. Am. Chem. Soc.* **2008**, *130*, 2922−2923.
(30) Wang, X.-Y.; Wang, L.; Wang, Z.-M.; Su, G.; Gao, S. *Chem. Mater.* **2005**, *17*, 6369−6380.
(31) Addison, A. W.; Rao, T. N.; Reedijk, J.; Rijn, J. v.; Verschoor, G. C. *J. Chem. Soc., Dalton Trans.* **1984**, 1349−1356.
(32) Blatov, V. A.; Shevchenko, A. P. *TOPOS 4.0*; Samara State University, Samara Oblast, Russia, 2008.